Progress In Electromagnetics Research B, Vol. 42, 225–243, 2012

LEAST SQUARES FILTERING ALGORITHM FOR REACTIVE NEAR FIELD PROBE CORRECTION

M. A. Moutaouekkil[1, *], A. Ziyyat[1], M. Serhir[2], and D. Picard[2]

[1]Electronic and Systems Laboratory, Faculty of Sciences, Mohammed 1th University, Oujda 60000, Morocco

[2]DRE, Laboratoire des Signaux et Systèmes (UMR 8506: Supelec CNRS-Univ. Paris-Sud 11), SUPELEC 3 Rue Joliot-Curie, Gif-sur-Yvette 91192, Cedex, France

Abstract—The probe correction technique applied to reactive near field characterization is based on a deconvolution process. However, the classical deconvolution based on an inverse Fourier transform has a restrictive limitation. It is based on the use of noiseless measurement data. Consequently, measurement noise makes the result obtained by the classical deconvolution based technique inefficient and requires an extremely low noise measurement facility. In this paper, a method to improve the probe correction stability when using corrupted measurement data is presented. The proposed constrained least squares filtering algorithm (CLSF) uses an inverse filtering approach that takes into account the statistical characteristics of the measurement noise. Computations data with electromagnetic software of two different structures validate this method and illustrate its reliability.

1. INTRODUCTION

Nowadays, technological progress allows high integration capacities by incorporating different electronic circuits with higher triggering frequencies in a limited area. The proximity between radio electronic devices has caused increasing electromagnetic interferences (EMI) which are difficult to diagnose with conventional near-field or far-field measurement systems. The measurement of the near-field emitted from electronic devices appears to be a promising

Received 4 June 2012, Accepted 11 July 2012, Scheduled 16 July 2012

* Corresponding author: Mohammed Anisse Moutaouekkil (anisse84@yahoo.fr).

approach in electromagnetic compatibility studies. Consequently, different mapping techniques have been developed to investigate the electromagnetic field in the immediate vicinity of the circuit under test to appreciate the electromagnetic interactions and find the appropriate solutions.

In classical near-field scanning for antenna measurements, the scanning plane is located outside the reactive near-field region of the antenna where the field energy due to the evanescent plane waves could be ignored. But in near-field scanning for a source reconstruction, the observation plane z is located much closer to the radiating object where the reactive energy of the field could not be neglected.

The near-field scanning technique has been used in various areas, from antenna analysis [1] to scanning of VLSI devices [2, 3], where possible applications ranging from pure emission hot-spot localization, via far-field and radiated emission estimation to reconstruction of the source distribution [4, 5].

Especially for the investigation of possible sources, e.g., detection of accumulated charge or the estimation of current paths, a high resolution, i.e., ability to distinguish closely separated sources in the scanned fields, is very important. Certainly, a point measurement would be ideal, but it is not possible due to the finite size of the measurement probe and its reaction with the field. However, the measured field is directly correlated with the used probe, and a post-processing step is needed to extract the field radiated by the device under test (DUT). This is called probe correction techniques. One of these methods is the complex deconvolution technique.

The complex deconvolution technique has been used in near-field probe correction in [6–9] in order to enhance the measurement data accuracy. Also, a high resolution characterization of the DUT emitted field requires the use of a small probe. Hence, a small probe possesses a lower sensitivity, and consequently, the measured data have a reduced signal to noise ratio. However, as presented in [6–9], authors have neglected the measurement noise contribution. This drawback makes the result obtained by the deconvolution method inefficient and requires the use of a very low noise measurement facility.

In this paper, we propose an improved deconvolution technique based on the inverse filtering approach that takes into account the apriori information concerning the statistical characteristics of measurement noise.

Using the constrained least squares filtering (CLSF) process [10], which has been applied successfully in digital image processing, we can guarantee the stability of the deconvolution technique when data are corrupted by noise. The CLSF process requires the knowledge of the

mean and the variance of the measurement noise. These parameters can be calculated easily from the measured signal.

2. METHOD

2.1. Deconvolution Method

The measured signal, collected by the probe $v(x, y, z, f)$ at the given height z and frequency f, is the result of the convolution of the exact field distribution $e(x, y, z, f)$ and the probe's response $h(x, y, z, f)$. The measured signal is possibly corrupted by the noise function $n(x, y, z, f)$ introduced during the measurement.

The test procedure is written as:

$$\begin{aligned} v(x,y,z,f) &= e(x,y,z,f) * h(x,y,z,f) + n(x,y,z,f) \\ &= \int_{-\infty}^{+\infty}\int_{-\infty}^{+\infty} e(x',y',z,f)h(x-x',y-y',z,f) \\ &\quad dx'dy' + n(x,y,z,f), \qquad \text{with} \qquad e \in \{e_x, e_y, e_z\}, \end{aligned} \tag{1}$$

where e_x, e_y, e_z represent electric field components. $e(x, y, z, f)$ can also represent the magnetic field.

The convolution product is evaluated in the spectral domain as a simple multiplication of two-dimensional Fourier transform of the respective functions. Equation (1) can be expressed in the spectral domain as:

$$\begin{aligned} V(kx,ky,kz,f) &= E(kx,ky,kz,f) \times H(kx,ky,kz,f) \\ &\quad + N(kx,ky,kz,f), \end{aligned} \tag{2}$$

where capital letters indicate the 2-D Fourier transforms of the corresponding spatial functions.

Many studies on this issue [6–9] have evaluated the DUT radiated field using direct inverse filtering (DIF) technique. The estimated field $E'(kx, ky, kz, f)$ is calculated by dividing the Fourier transform of the measured signal $V(kx, ky, kz, f)$ by the Fourier transform of the probe response $H(kx, ky, kz, f)$. Nevertheless, the DIF technique has been applied without taking into account the measurement noise.

Determining the field $E(kx, ky, kz, f)$ from Equation (2) shows that:

$$\begin{aligned} E'(kx,ky,kz,f) &= \frac{V(kx,ky,kz,f)}{H(kx,ky,kz,f)} - \frac{N(kx,ky,kz,f)}{H(kx,ky,kz,f)} \\ &= E(kx,ky,kz,f) - \frac{N(kx,ky,kz,f)}{H(kx,ky,kz,f)}. \end{aligned} \tag{3}$$

Equation (3) illustrates that even if the probe response is well known, we cannot accurately determine the exact DUT radiated field $E(kx,\ ky,\ kz,\ f)$. Indeed, the impact of measurement noise can become important for the case where $H(kx,\ ky,\ kz,\ f)$ takes very small values.

In this work, we solve this problem by an inverse filtering approach that integrates the statistical characteristics of noise using the constrained least squares filtering technique (CLSF) [10]. This method requires the knowledge of the mean and the variance of the noise. This is an important advantage over other types of inverse filtering that require the knowledge of the power spectral density of noise (Wiener filter) [10] in the sense that these parameters (mean and variance) can be evaluated easily for all measurement setup.

By using the definition of convolution we can express Eqution (1) in vector matrix from [10, 11]:

$$\widetilde{v} = \widetilde{H}\widetilde{e} + \widetilde{n} \tag{4}$$

$\widetilde{v}$ and $\widetilde{e}$ are respectively the voltage $v(x, y, z, f)$ and the field $e(x, y, z, f)$ written as a vector by stacking its columns one under the other. So $\widetilde{v}$ and $\widetilde{e}$ are matrices of size $N^2 \times 1$, where N is the number of points along x and y directions.

$$\begin{pmatrix} v(0,0) \\ v(1,0) \\ \vdots \\ v(N-1,0) \\ v(0,1) \\ v(1,1) \\ \vdots \\ v(N-1,1) \\ v(0,2) \\ v(1,2) \\ \vdots \\ v(N-1,2) \\ v(0,N-1) \\ v(1,N-1) \\ \vdots \\ v(N-1,N-1) \end{pmatrix} = \widetilde{H} \begin{pmatrix} e(0,0) \\ e(1,0) \\ \vdots \\ e(N-1,0) \\ e(0,1) \\ e(1,1) \\ \vdots \\ e(N-1,1) \\ e(0,2) \\ e(1,2) \\ \vdots \\ e(N-1,2) \\ e(0,N-1) \\ e(1,N-1) \\ \vdots \\ e(N-1,N-1) \end{pmatrix} + \begin{pmatrix} n(0,0) \\ n(1,0) \\ \vdots \\ n(N-1,0) \\ n(0,1) \\ n(1,1) \\ \vdots \\ n(N-1,1) \\ n(0,2) \\ n(1,2) \\ \vdots \\ n(N-1,2) \\ n(0,N-1) \\ n(1,N-1) \\ \vdots \\ n(N-1,N-1) \end{pmatrix} \tag{5}$$

$\widetilde{H}$ is a square $N^2 \times N^2$ block circulant matrix that is made up of $N \times N$

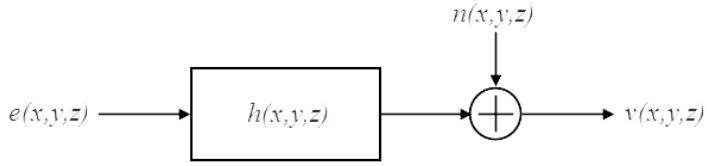

Figure 1. Test procedure: Relation between e and v.

submatrix of size $N \times N$ each, arranged in the following way:

$$\widetilde{H} = \begin{pmatrix} \begin{matrix} x' \rightarrow \\ x \downarrow \begin{pmatrix} y'=0 \\ y=0 \end{pmatrix} \end{matrix} & \begin{matrix} x' \rightarrow \\ x \downarrow \begin{pmatrix} y'=1 \\ y=0 \end{pmatrix} \end{matrix} & \cdots \begin{matrix} x' \rightarrow \\ x \downarrow \begin{pmatrix} y'=N-1 \\ y=0 \end{pmatrix} \end{matrix} \\ \begin{matrix} x' \rightarrow \\ x \downarrow \begin{pmatrix} y'=0 \\ y=1 \end{pmatrix} \end{matrix} & \begin{matrix} x' \rightarrow \\ x \downarrow \begin{pmatrix} y'=1 \\ y=1 \end{pmatrix} \end{matrix} & \cdots \begin{matrix} x' \rightarrow \\ x \downarrow \begin{pmatrix} y'=N-1 \\ y=1 \end{pmatrix} \end{matrix} \\ \vdots & \vdots & \vdots \\ \begin{matrix} x' \rightarrow \\ x \downarrow \begin{pmatrix} y'=0 \\ y=N-1 \end{pmatrix} \end{matrix} & \begin{matrix} x' \rightarrow \\ x \downarrow \begin{pmatrix} y'=1 \\ y=N-1 \end{pmatrix} \end{matrix} & \cdots \begin{matrix} x' \rightarrow \\ x \downarrow \begin{pmatrix} y'=N-1 \\ y=N-1 \end{pmatrix} \end{matrix} \end{pmatrix} \quad (6)$$

In this representation, each bracketed expression represents $N \times N$ submatrix made up from function $h(x - x', y - y')$ for fixed values of y and y' and with variables x and x' taking up all their possible values in the directions indicated by the arrows. The CLSF has its roots in a matrix formulation of Equation (4).

The principle of the CLSF method is to impose a smoothness constraint to the solution. Let us say that we would like the second derivative of the reconstructed field to be small overall. At each position, the second derivative of the field can be written as [10]:

$$\nabla^2 e'(x,y) = e'(x,y-1) + e'(x+1,y) + e'(x,y+1) - 4e'(x,y) \quad (7)$$

This is the expression of the Laplacian at position (x, y). The constraint that we choose to impose is to minimize the sum of the squares of the Laplacian values at each position Equation (8) :

$$\sum_{x=0}^{N-1} \sum_{y=0}^{N-1} \left| \nabla^2 e'(x,y) \right|^2 \quad (8)$$

The value of the Laplacian at each position can be computed by the Laplacian operator L which has the form of an $N^2 \times N^2$ block circulant matrix acting on the column vector $\widetilde{e'}$. The sum of the squares

of its elements is given by $(L\widetilde{e'})^T \cdot (L\widetilde{e'})$. The constraint is to minimize the quantity [11]:

$$(L\widetilde{e'})^T \cdot (L\widetilde{e'}) \tag{9}$$

We assume that the noise vector $\widetilde{n}$ is not known but some of his statistical properties are known; say we know that:

$$\widetilde{n}^T \cdot \widetilde{n} = \varepsilon \tag{10}$$

This quantity ε is related to the variance of noise. If we substitute $\widetilde{n}$ from (4) into (10) we have:

$$(\widetilde{v} - \widetilde{H}\widetilde{e'})^T \cdot (\widetilde{v} - \widetilde{H}\widetilde{e'}) = \varepsilon \tag{11}$$

According to the method of Lagrange multipliers, the solution must satisfy:

$$\frac{\partial}{\partial \widetilde{e'}} \left[\widetilde{e'}^T L^T L \widetilde{e'} + \lambda \left(\widetilde{v} - \widetilde{H}\widetilde{e'} \right)^T \left(\widetilde{v} - \widetilde{H}\widetilde{e'} \right) \right] = 0, \tag{12}$$

where λ is a constant.

To solve this equation we need some mathematical properties of vectors and block circulant matrix. We present the mathematical details in the appendix.

We apply the property 1 to Equation (12) to perform the differentiation:

$$\widetilde{e'} = [\widetilde{H}^T \widetilde{H} + \beta L^T L]^{-1} \widetilde{H}^T \widetilde{v}, \tag{13}$$

where $\beta = \frac{1}{\lambda}$.

We apply the property 2 to Equation (12) to get:

$$(\Lambda_h^* \Lambda_h + \beta \Lambda_1^* \Lambda_1) W^{-1} \widetilde{e'} = \Lambda_h^* W^{-1} \widetilde{v} \tag{14}$$

Finally, the application of the property 3 gives the expression of the spectral domain solution for CLSF method:

$$E'(kx, ky) = \left[\frac{H^*(kx, ky)}{|H(kx, ky)|^2 + \beta |L(kx, ky)|^2} \right] V(kx, ky), \tag{15}$$

where $H^*(kx, ky)$ is the complex conjugate of $H(kx, ky)$.

β is a parameter to be adjusted, and in practice, it can be estimated by [12]:

$$\beta = \frac{\sigma_n^2}{\sigma_v^2 - \sigma_n^2}, \tag{16}$$

where σ_n^2 is the measurement noise variance and σ_v^2 the measured signal $v(x, y)$ variance.

2.2. Test Procedure

In order to verify the efficiency of the Constrained Least Squares Filtering Method compared with the Direct Inverse Filtering technique, we consider a situation for which the actual device under test radiated electric field and the exact probe model are fully known. In fact, we calculate the voltage $v(x, y, z)$ by a direct convolution product between the mathematical function representing the probe response $h(x, y, z)$ and the normal electric field radiated by the Device Under Test determined using a simulation software. Thereafter, a controlled noise $n(x, y)$ with a given variance value is added to the calculated voltage $v(x, y, z)$.

Based on the noisy voltage $v(x, y, z)$, we estimate the field $e'(x, y, z)$ using CLSF and DIF methods respectively. The resulting $e'(x, y, z)$ issued from each method and associated to different noise levels is compared with the actual field $e(x, y, z)$. This verification procedure is schemed in Fig. 2.

2.3. The Probe Response and Tested Structures

As mentioned before, for the verification procedure we have to define a well-known probe. The chosen probe is a semi-rigid coaxial cable. This probe is well adapted for measuring the normal electric field. This probe was used because of its popularity in near-field measurements and for its structural simplicity, being easily modeled in

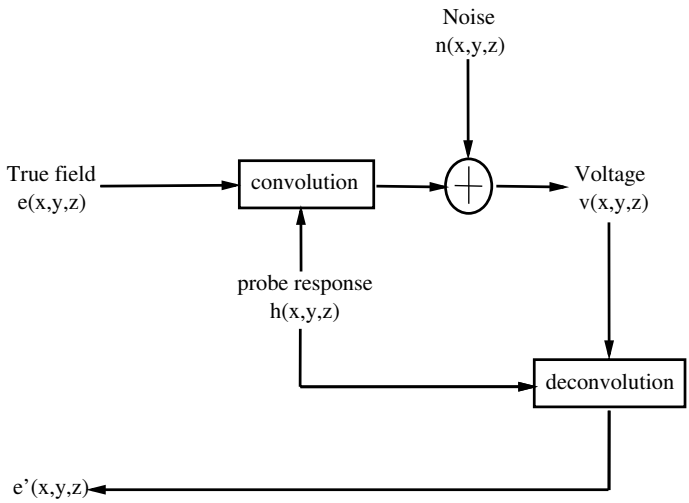

Figure 2. Schematic test procedure.

any electromagnetic field solver. Such a basic probe without extension of the inner conductor of the semi-rigid coaxial cable provides a good resolution and a high magnetic to electric field rejection in the near-field region. This probe is modeled by a simple mathematical function as a Ricker wavelet weighted by a factor a [9, 13]. The considered function is expressed in (17) and presented in Fig. 3.

$$h(x,y) = \left(1 - 2\Pi^2 a^2 (x^2+y^2)\right) \exp\left(-\Pi^2 a^2 (x^2+y^2)\right) \exp\left(-\jmath k (z^2+x^2+y^2)^{1/2}\right) \quad (17)$$

The factor a depends on the dimensions of the probe and the height z.

Furthermore, to validate this probe correction method, the study is performed for two different devices under test (DUT). The first DUT is a patch antenna where the rate of change in normal electric field is smooth due to the fact that the electric charges are distributed over a large circular area. The second structure is a quadrature hybrid coupler. This device radiates a very concentrated normal electric field above relatively narrow strips.

The two DUT (patch antenna and coupler) are etched on a standard epoxy FR4 laminate in a microstrip technique. The geometric characteristics of both structures are detailed in Fig. 4.

The structures are simulated using CST Microwave Studio at the frequency of 1 GHz [14]. Then, the computed normal component of the electric field, $e_z(x,y)$, is determined within a rectangular plane of size $100 * 100\,\mathrm{mm}^2$. This size is chosen large enough to obtain very low field at the edges of this scanning plane to prevent any support truncation error during multiple processing. The measurement plane is located at $z = 1\,\mathrm{mm}$ above their upper surface. The $e_z(x,y)$ field is sampled every 0.5 mm in both directions x and y.

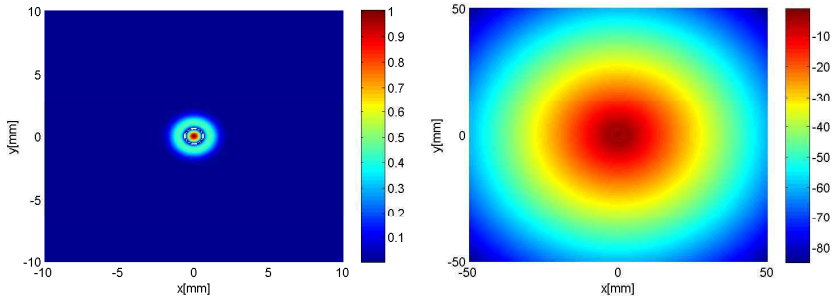

Figure 3. 2D probe's response. (a) Normalized amplitude and (b) phase [deg] for frequency = 1 GHz and $z = 1\,\mathrm{mm}$.

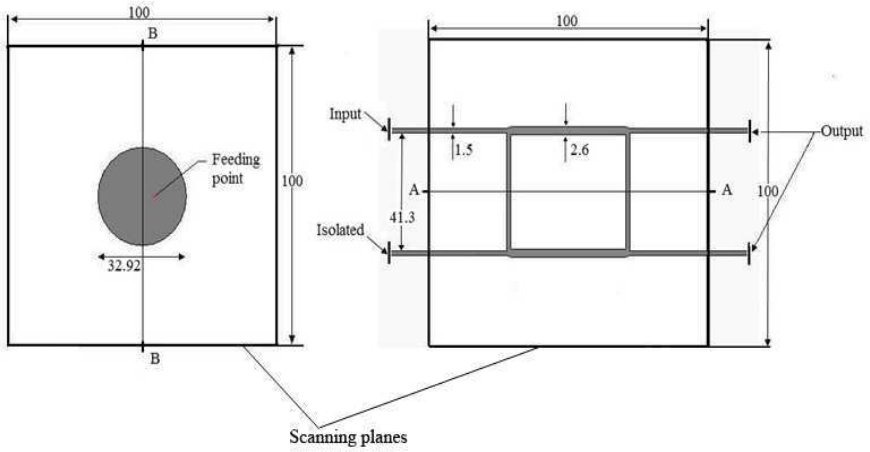

Figure 4. Scanning planes and cross-sections of the test structures.

Table 1. Levels of noise variance added to $v(x, y)$ (dB) and those retrieved $e(x, y)$ using the two methods for DIF and CLSF for two DUTs at a measurement height of $z = 1\,\text{mm}$ and a frequency $f = 1\,\text{GHz}$.

		signal to noise ratio (dB) on $e'(x, y)$			
		patch antenna		**hybrid coupler**	
noise level (dB)	β	DIF	CLSF	DIF	CLSF
-100	$5.2\ 10^{-5}$	-39	-60	-40	-64
-80	$5.18\ 10^{-4}$	-19	-50	-21	-48
-60	0.0052	-11	-41	-11	-37
-40	0.051	-10	-30	-10	-30

3. RESULTS

As can be seen from Table 1, using a DIF technique, a small perturbation on the voltage signal $v(x, y)$ generates a large disturbance on the reconstructed field, in such a way, we totally loose the field characteristics for an added noise level of $-60\,\text{dB}$ (Fig. 5(c), Fig. 6(c), Fig. 7(c) and Fig. 8(c)).

Also, using the CLSF technique, the effect of the added noise has been controlled for both DUTs. As presented in Fig. 5, Fig. 6, Fig. 7 and Fig. 8, for an added noise level of $-60\,\text{dB}$, the reconstructed field has an average 2D error less than $-37\,\text{dB}$. Visually, it is a very satisfactory reconstructed field compared with the DIF technique

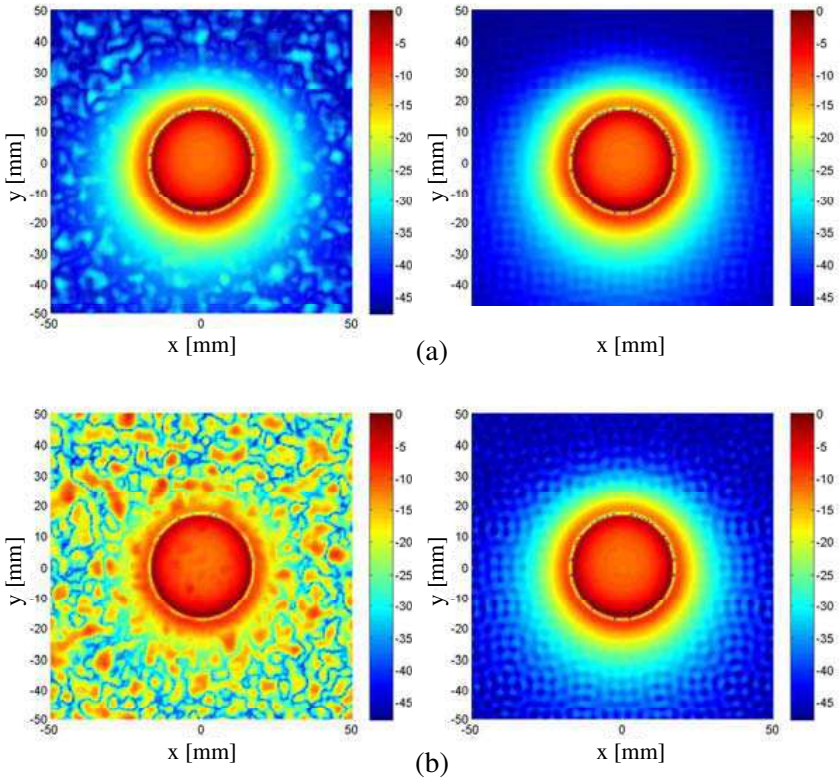

results.

In Table 1, we present the β value corresponding to each added noise level. In order to verify the stability of $e'(x, y)$ reconstruction as a function of β variation, we have considered the case for which the added noise level is -60 dB.

From Table 1, an added noise level of -60 dB corresponds to $\beta = 0.0052$ (this value is given by the Equation (16). For -20% of the β initial value the CLSF technique leads to $+2.5\%$ variation of the reconstructed field noise level. For $+20\%$ of the initial β value the CLSF technique leads to -4.5% variation of the reconstructed field noise level.

Figure 9 shows the distribution of the field in the cross sections A-A and B-B defined in Fig. 4 for both DUTs. We note that the method CLSF greatly improves the field reconstruction compared with DFI method and allows us to obtain good results for noise levels between -100 dB and -50 dB and even average results for a level noise of -40 dB for both DUTs.

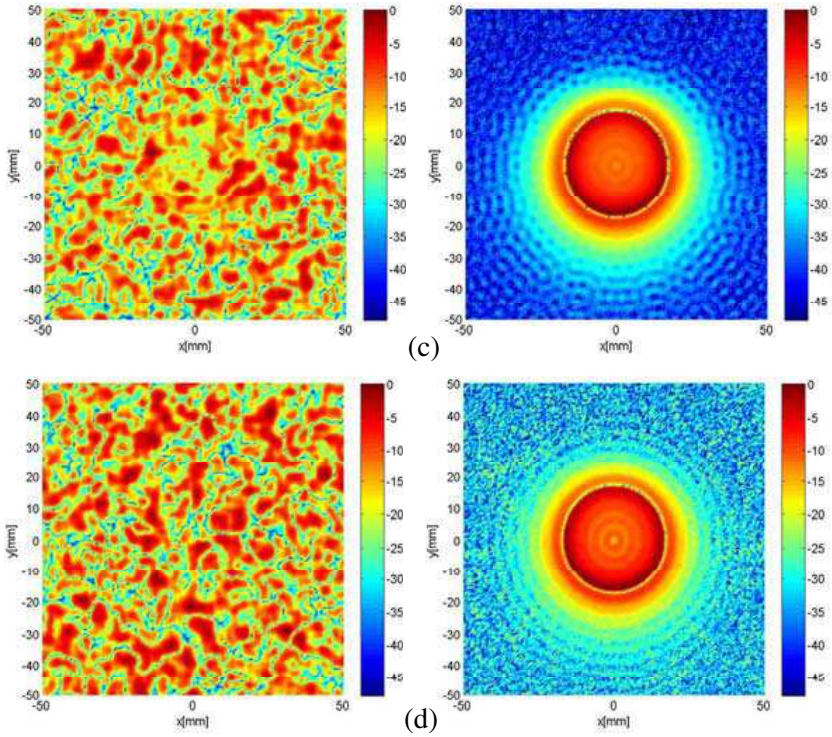

Figure 5. The normalized amplitude [dB] of the normal electric field radiated by the patch antenna calculated by DIF and CLSF methods, for different noise levels. (a) −100 dB. (b) −80 dB. (c) −60 dB and (d) −40 dB (left) DIF and (right) CLSF.

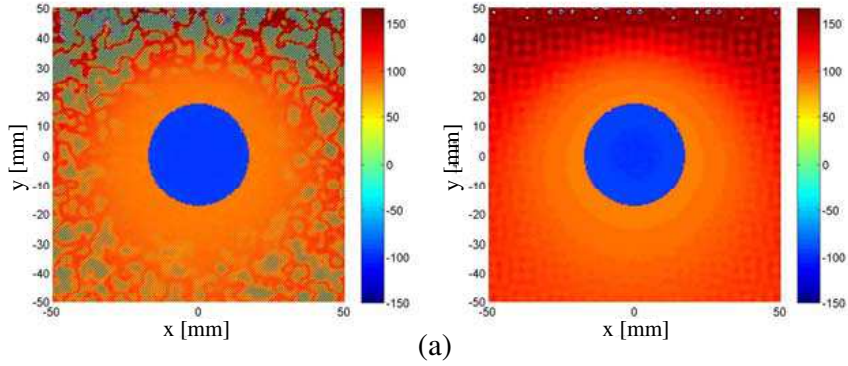

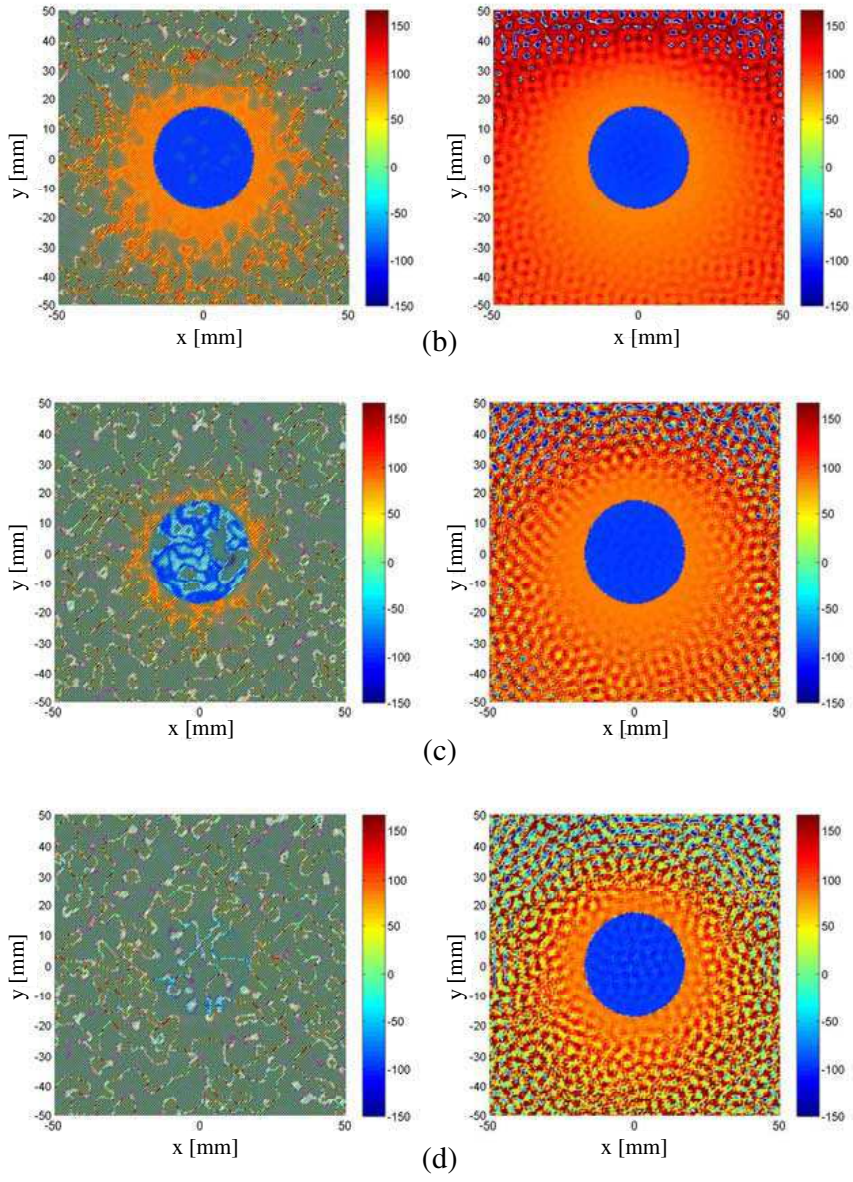

Figure 6. The phase [deg] of the normal electric field radiated by the patch antenna calculated by DIF and CLSF methods, for different noise levels. (a) −100 dB. (b) −80 dB. (c) −60 dB and (d) −40 dB (left) DIF and (right) CLSF.

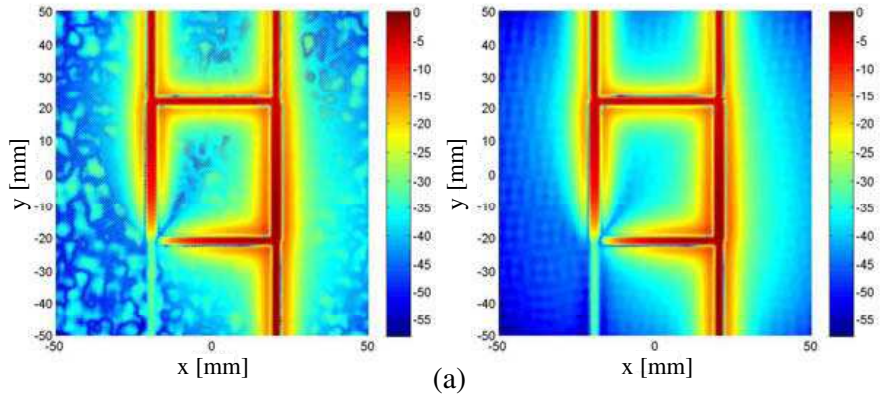
y [mm]
x [mm]
50
40
30
20
10
0
-10
-20
-30
-40
-50
-50
0
50
0
-5
-10
-15
-20
-25
-30
-35
-40
-45
-50
-55

(a)

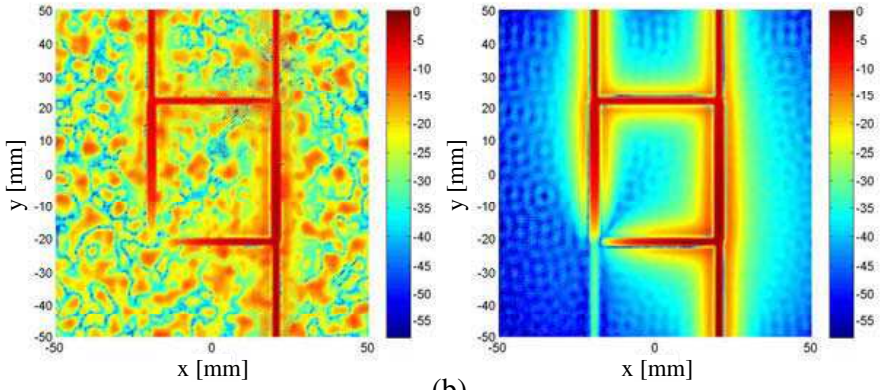
y [mm]
x [mm]
50
40
30
20
10
0
-10
-20
-30
-40
-50
-50
0
50
0
-5
-10
-15
-20
-25
-30
-35
-40
-45
-50
-55

(b)

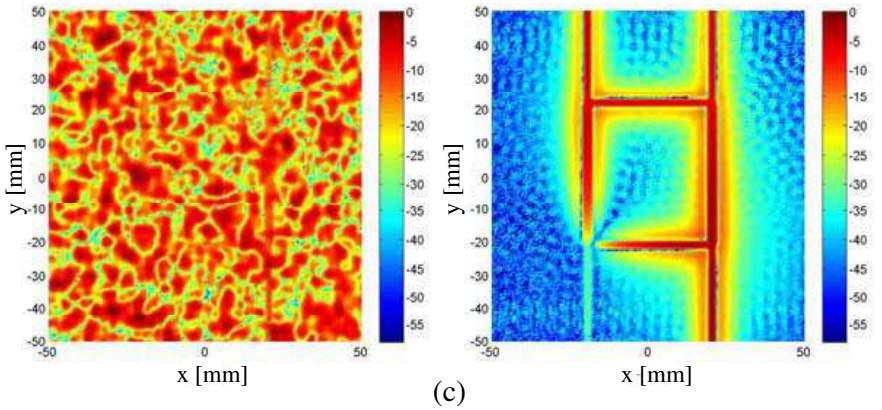
y [mm]
x [mm]
50
40
30
20
10
0
-10
-20
-30
-40
-50
-50
0
50
0
-5
-10
-15
-20
-25
-30
-35
-40
-45
-50
-55

(c)

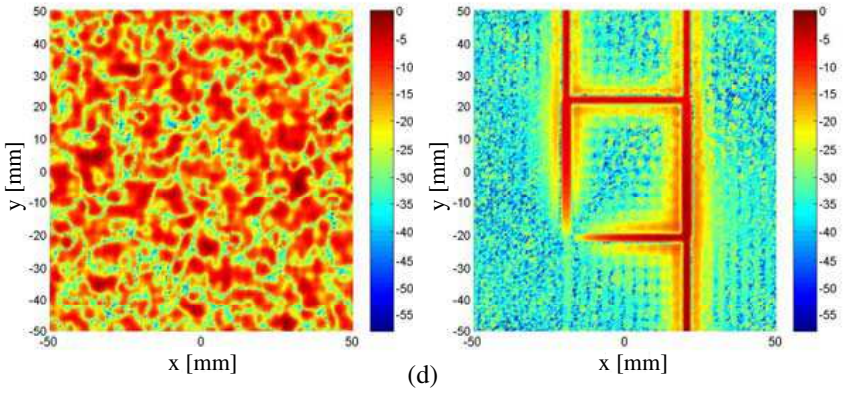

Figure 7. The normalized amplitude [dB] of the normal electric field radiated by the hybrid coupler calculated by DIF and CLSF methods, for different noise levels. (a) −100 dB. (b) −80 dB. (c) −60 dB and (d) −40 dB (left) DIF and (right) CLSF.

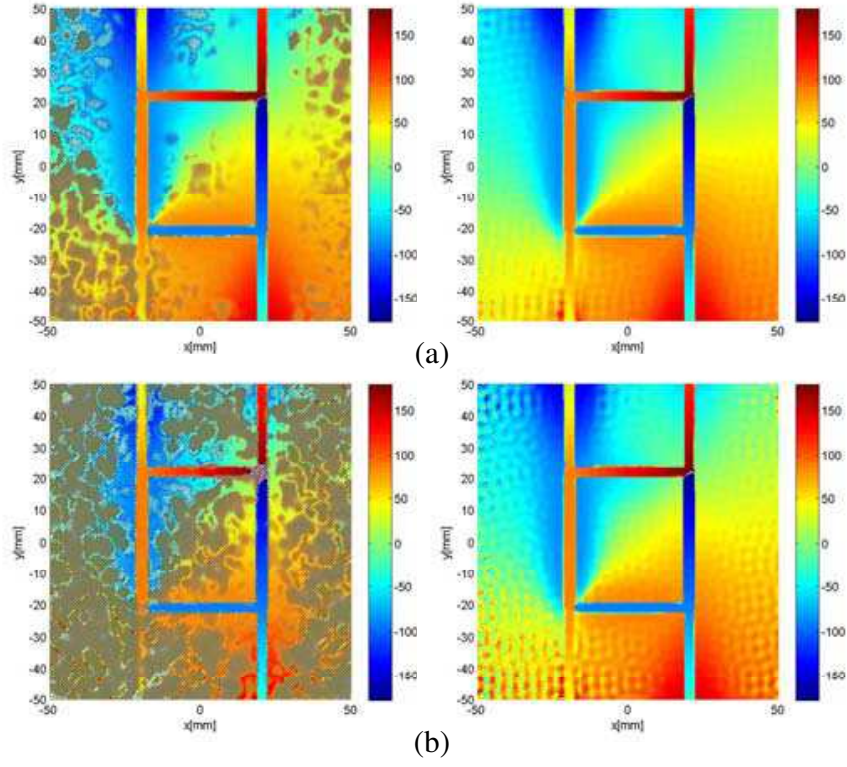

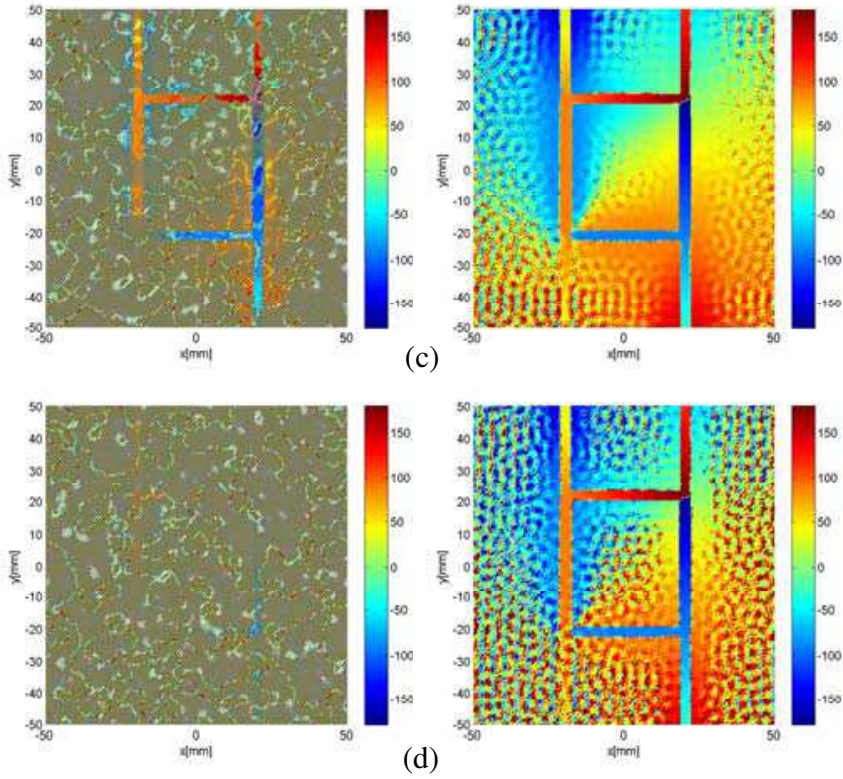

Figure 8. The phase [deg] of the normal electric field radiated by the hybrid coupler calculated by DIF and CLSF methods, for different noise levels. (a) −100 dB. (b) −80 dB. (c)−60 dB and (d) −40 dB (left) DIF and (right) CLSF.

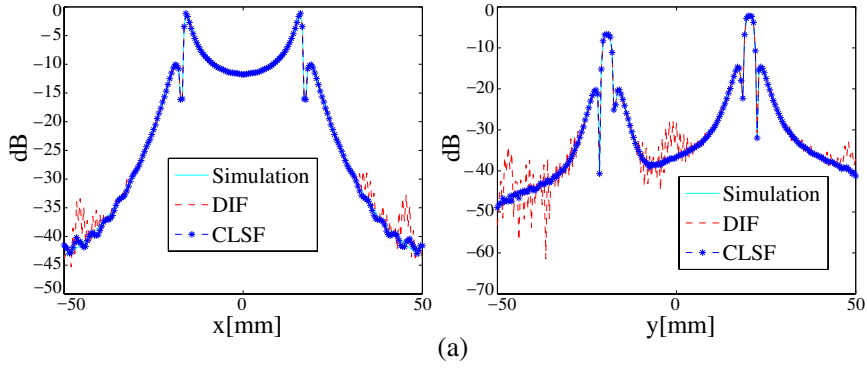

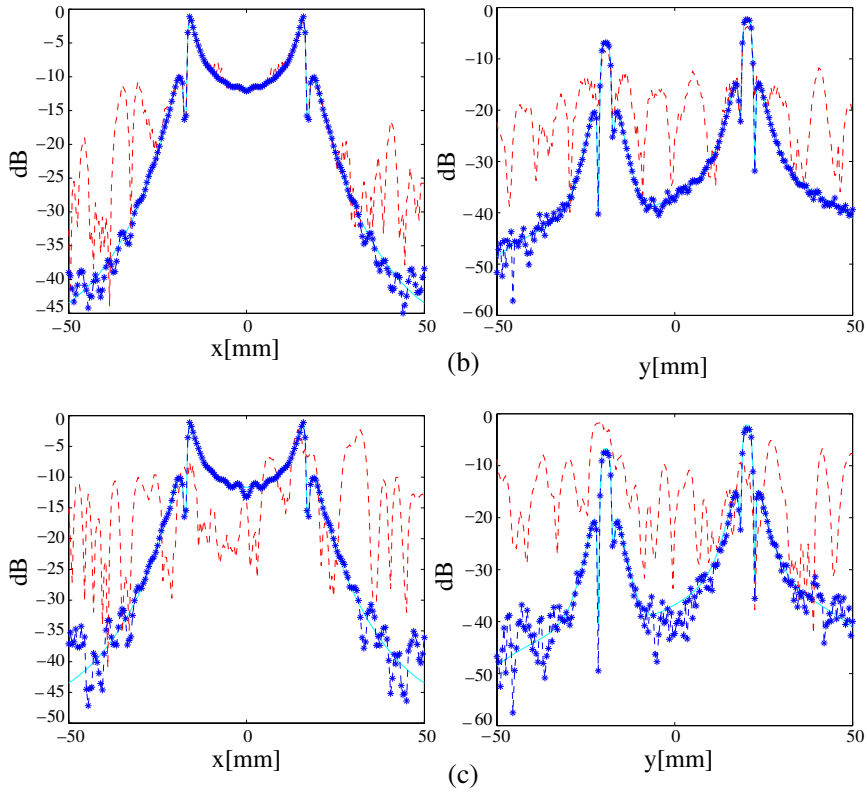

Figure 9. The normalized amplitude [dB] of the normal electric eld radiated by the both DUTs in the cross section A-A and B-B calculated by DIF and CLSF methods, for different noise levels. (a) −100 dB. (b) −80 dB and (c) −60 dB.

4. CONCLUSION AND PERSPECTIVE

In this work, we have shown that the classical deconvolution technique for probe correction based on direct inverse filtering (DIF) presents some limitations caused by the presence of the measurement noise. Consequently, a filtering technique has been proposed to overcome this limitation. Based on constrained least squares filtering, the correction method proposed in this paper has shown a good ability to limit strongly the effect of noise and given very satisfactory results even for high level of noise. In addition, this method presents a high stability and requires only the noise statistical characteristics, which are easily obtained from the measurement setup. The CLSF can be applied to any electromagnetic near-field probe when its spectral response takes

small values. This correction was performed with a single polarization of the probe response. For full near-field probe correction, we will investigate the effect of multi-polarized probe taking into account the near-field coupling effect between the probe and the DUT.

APPENDIX A. PROPERTY 1

If a and b are vectors and A a square matrix, then it can be shown that:

$$\frac{\partial \widetilde{e'}^T a}{\partial \widetilde{e'}} = a. \tag{A1}$$

$$\frac{\partial b^T \widetilde{e'}}{\partial \widetilde{e'}} = b. \tag{A2}$$

$$\frac{\partial \widetilde{e'}^T A \widetilde{e'}}{\partial \widetilde{e'}} = (A + A^T)\widetilde{e'}. \tag{A3}$$

APPENDIX B. PROPERTY 2

Let M be a block circulant matrix of size $N^2 \times N^2$. Based on [11], M can be written as:

$$M = W \Lambda_m W^{-1}, \tag{B1}$$

where

$$W = W_N \otimes W_N, \quad \text{with} \quad W_N(k,n) = \frac{1}{\sqrt{N}} \exp\left(\frac{2\Pi j}{N} kn\right). \tag{B2}$$

The operator $\otimes$ is the Kronecker product of the two matrices and Λ_m expressed as:

$$\Lambda_m(x,y) = \begin{cases} N \cdot M(kx,ky) & \text{if} \quad x = y. \\ 0 & \text{if} \quad x \neq y, \end{cases} \tag{B3}$$

where $M(kx,ky)$ is the Fourier transform of matrix M. We note that the columns of W are the eigenvectors of matrix M.

APPENDIX C. PROPERTY 3

We have the following result [11]:

$$W^{-1} v = V(kx,ky) \tag{C1}$$

$$\Lambda_1^* \Lambda_1 = N^2 |L(kx,ky)|^2 \tag{C2}$$

where v is a vector of dimension $N^2 \times 1$. V and L are, respectively, the Fourier Transform of the vector v and the Kernel function $l(x, y)$. l is the Kernel function of the Laplacian operator L, expressed as:

$$l(x,y) = \begin{pmatrix} 0 & -1 & 0 \\ -1 & 4 & -1 \\ 0 & -1 & 0 \end{pmatrix} \tag{C3}$$

REFERENCES

1. Slater, D., *Near-Field Antenna Measurements*, Artech House, Boston, London, 1991.
2. Slattery, K., J. W. Neal, and W. Cui, "Near-field measurements of VLSI devices," *IEEE Trans. on Electromagnetic Compatibility*, Vol. 41, No. 4, 374–384, November 1999.
3. Tankielun, A., P. Kralicek, U. Keller, E. Sicard, and B. Vrignon, "Influence of core optimisation and activity for electromagnetic near-field and conducted emissions of CESAME test chip," *4th International Workshop on Electromagnetic Compatibility of Integrated Circuits*, No. 4, 95–100, 2004.
4. Las-Heras, F. and T. K. Sarkar, "A direct optimization approach for source reconstruction and NF-FF transformation using amplitude-only data," *IEEE International Symposium on EMC*, Vol. 50, No. 4, 500–510, 2002.
5. Sarkar, T. K. and F. Las-Heras, "An iterative spherical near-field to far-field emissions and source reconstruction using the equivalent current approach," *IEEE International Symposium on EMC*, Vol. 1, 395–398, 2001.
6. Riah, Z., D. Baudry, M. Kadi, A. Louis, and B. Mazari, "Post-processing of electric field measurements to calibrate a near-field dipole probe," *IET Sci. Meas. Technol*, Vol. 5, No. 2, 29–36, 2011.
7. Tankielun, A., U. Keller, W. John, and H. Garbe, "Complex deconvolution for improvement of standard monopole near-field measurement results," *16th Int. Zurich Symp., EMC200*, Zurich, 2005.
8. Shi, J., M. A. Cracraft, K. P. Slattery, M. Yamaguchi, and R. E. DuBroff, "Calibration and compensation of near-field scan measurements," *IEEE Journal on Electromagnetic Compatibility*, Vol. 47, No. 3, 642–650, 2005.
9. Bouchlouk, L., "Conception et validation de sondes pour les mesures en champ proches," Ph.D. Thesis, University Pris sud XI, 2006.

10. Gonzales, R. C. and R. E. Woods, *Digital Image Processing*, Addison-Wesley Publishing Company, PAYS, 1993.
11. Petrou, M. and P. Bostogianni, *Image Processing: The Fundamentals*, Wiley, UK, 1999.
12. Yeoh, W. S. and C. Zhang, "Constrained least squares filtering algorithm for ultrasound image deconvolution," *IEEE Transactions on Biomedical Engineering*, Vol. 53, No. 10, 2001–2007, 2006.
13. Schneider, B., "Plane waves in FDTD simulations and a nearly perfect total-field/scattered-field boundary," *IEEE Transactions on Antennas and Propagation*, Vol. 52, No. 12, 3280–3287, 2004.
14. CST, GmbH, "From design to reality," *Microwave Journal*, Vol. 47, No. 1, 2004.